

Modelling the Drying of Porous Coal Particles in Superheated Steam

B. A. Olufemi* and I. F. Udefiagbon

Department of Chemical Engineering,
University of Lagos, Akoka, Nigeria

Original scientific paper

Received: July 21, 2008

Accepted: June 1, 2009

The modelling and simulation of drying porous coal particles in superheated steam was investigated in this paper. Improved transport and kinetic parameters as well as particle shrinkage were considered in arriving at the results. The resulting partial differential equation describing the drying process was solved numerically using the finite element analysis in addition to other useful equations. This is an improvement over the finite difference analysis that some previous researchers have been using. The simulated results obtained showed very reliable results, as experimental results were properly matched. This is very good justification that the model considerations as well as the good mathematical analysis of the drying process undoubtedly led to a better understanding of the process. This will aid future researchers to design better experiments, equipment and products.

Key words:

Modelling, simulation, coal, particle, drying

Introduction

The several advantages that superheated steam drying has over hot air drying have made it a centre of attraction. First the quantity of gas to be handled is lower thereby reducing handling costs, while the latent heat of evaporation could be recovered and reused, thereby rendering the process more thermally efficient at a reduced cost. Wet coal particles have to be dried prior to combustion or gasification in order to generate energy with improved thermal efficiency. Drying of coal can significantly increase its value, with less maintenance of plant equipment, while the quantity of stack emissions, net plant heat rate and auxiliary power needed can be reduced substantially.

The subject of drying in superheated steam has been in discussion since 1908.¹ However, significant industrial application of the process occurred in 1920.² Various researchers have done characterisation and experimental observation on the kinetics of drying coal particles in superheated steam. Experiments ranging from drying a single coal particle, fixed bed of coal particles, as well as fluidized bed of coal particles are available in the literature. There are however varying investigations from different researchers about the mechanism of the drying process. Various drying models have been proposed over the years with a view to properly explain the kinetics and dynamics of the drying process.³ In another similar recent study, Edward *et al.* in 2006 presented experimental and theoretical in-

vestigation on the kinetics of coal drying in a fluidized bed.⁴

In this paper, a mathematical model was developed for Victorian lignite coal with a typical raw moisture content of about 60 %. A single porous lignite coal particle was the subject of investigation with a view that a proper analysis of the particle will enable a better understanding of more industrial applications. The models were validated with the experimental results proposed by Looi *et al.*³ which also analysed the kinetics of single coal drying in superheated steam.

Mathematical modelling of the drying process

Two mechanistic models are available in the literature for the drying process. One of the models assumes that the temperature of the particle surface is expected to rise at the same time as that of the particle core (centre), as proposed by Hager *et al.* in 1997.⁵ The second model, on the other hand, assumes that evaporation occurs only at the drying front that recedes from the particle surface to the core as drying progresses. The latter is usually known as the receding core model and has been investigated by Shibata *et al.* in 1988,⁶ Khan *et al.* in 1991⁷ and Moyne *et al.* in 1990.⁸

This work assumes the receding core model that evaporation occurs only at the drying front that recedes from the particle surface to the core. It is assumed that the drying front assumes a singular saturated condition, the wet zone between the core

*Author for correspondence: email: bolufemi@yahoo.com,
Tel: + 234 802 316 2183

and the drying front remains below the steam saturated temperature, while the temperature of the dry zone approaches the surrounding hot temperature as time progresses.

In deriving the model equations for the system, mass transfer resistance to the drying of the particle as idealised in Fig. 1 is assumed negligible. Evaporation of moisture only takes place at the drying front. At the prevailing temperature considered throughout, heat transfer by radiation is also considered negligible. Sequentially, heat is transferred from the surrounding superheated steam by convection while the entire wet particle temperature remains below the saturated steam temperature at the prevailing pressure during the initial preheating period.

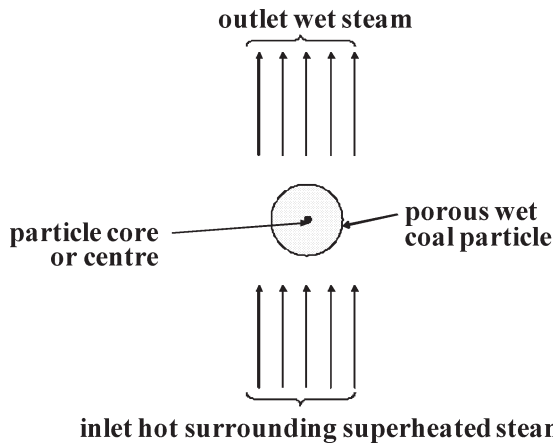


Fig. 1 – Schematic view of the coal drying operation

Within the particle, the sole mode of heat transfer is considered to be by conduction by the solid matrix and within the pores of the particle. An energy balance on the particle can be represented as:

$$\text{heat input} - \text{heat output} + \text{heat generated} - \text{heat consumed} = \text{heat accumulated} \quad (1)$$

$$\text{heat generated} = \text{heat consumed} = 0 \quad (2)$$

Considering an elemental portion of the particle between radii r and $r + \Delta r$

$$\begin{aligned} \Rightarrow & (2\pi r \Delta Z h T_r - 2\pi r \Delta Z h T_{r+\Delta r}) + \\ & + (2\pi r \Delta Z J_r - 2\pi r \Delta Z J_{r+\Delta r}) = \quad (3) \\ & = \rho c_p 2\pi r \Delta r \Delta Z \frac{\partial T}{\partial t} \end{aligned}$$

The first bracket on the left hand side (LHS) of eq. (3) represents the convective heat flow between input and output, while the second bracket on the LHS represent that of the conductive heat flow respectively. The right hand side (RHS) of eq. (3) is the heat accumulated.

Taking limits and simplifying further,

$$\Rightarrow -h \frac{\partial T}{\partial r} + \frac{1}{r} \frac{\partial}{\partial r} \left(k \frac{\partial T}{\partial r} \right) = \rho c_p \frac{\partial T}{\partial t} \quad (4)$$

Expanding, dividing by $\rho \cdot c_p$ and simplifying further, we see that,

$$\frac{\partial T}{\partial t} = -m \frac{\partial T}{\partial r} + \alpha \left\{ \frac{1}{r} \frac{\partial T}{\partial r} + \frac{\partial^2 T}{\partial r^2} \right\} \quad (5)$$

where,

$$\alpha = \frac{\kappa}{\rho c_p} \text{ and } m = \frac{h}{\rho c_p}$$

As convective heat transfer within the particle is negligible, m tends to zero.

The temperature profile is assumed to be symmetric about the centre of the particle whose temperature is assumed to rise slower than that of the surface. This generates a temperature gradient within the particle that gradually approaches a thermal equilibrium state. At the surface of the particle however, the temperature gradient is assumed to be linear. The following boundary conditions govern the limits of the operation:

$$\frac{\partial T}{\partial r} = 0 \text{ for } r = 0 \quad (6)$$

$$\kappa \frac{\partial T}{\partial r} = h(T_h - T) \text{ for } r = r_p \neq r_f \quad (7)$$

It is assumed that as drying progresses, the heat transferred to the drying front is solely used for evaporation. Also, drying progresses at the drying front until the moisture content of the particle at that point falls from the initial moisture content w_i to the final moisture content w_f . As w_f is reached, the drying front moves toward the core again while the dry zone temperature continues to rise towards T_h . This continues until the drying front recedes to the core.

The evaporation of moisture at the drying front can be modelled as:

$$q_w = \frac{h A_f (T_h - T_s)}{h_{lg}}, \text{ for } r = r_f = r_p \quad (8)$$

T_h is the operating temperature of the hot surrounding air, which is usually higher than the prevailing steam saturation temperature, T_s .

$$q_w = \frac{\kappa A_f \left(\frac{\partial T}{\partial r} \right)}{h_{lg}}, \text{ for } r = r_f \neq r_p \quad (9)$$

Additionally considered in this study was the mathematical analysis of particle shrinking as drying progresses. This is based on the assumption that the voids created by the evaporated moisture will collapse and the particle shrink as observed by Looi *et al.* in 2002.³

This implies that:

$$V_f = V_i - \Delta V \quad (10)$$

where

$$\Delta V = \frac{q_w t}{\rho_1} \quad (11)$$

The transient particle radius is recalculated as follows:

$$r_t = \sqrt[3]{\frac{3V_f}{4\pi}} \quad (12)$$

The transient particle radius is recalculated continuously as the particle shrinks, and until drying is achieved when the transient moisture content has attained a constant value of the final (critical) moisture content and the drying front coincides with the particle core. The transient moisture content is given as

$$w_t = w_i - \frac{q_w t}{m_s} \quad (13)$$

Numerical solution

The partial differential equation in eq. (5) was solved with the finite element numerical method. This method utilised triangular mesh to approximate the temperature variation across the particle,

which is a very accurate method instead of using the finite difference method that approximates the solution with rectangular mesh. A triangular mesh approximation of the finite element method is compared below to that of a rectangular mesh.

As may be seen in Fig. 2, the triangular mesh generates more precise nodal points in order to give a more accurate numerical approximation of the particles especially at the particle surface. Triangular mesh regeneration also helped to improve the results accuracy.

Eq. (6) to eq. (12) was incorporated into the numerical solution technique, while the heat transfer coefficient between the bulk steam and particle surface was estimated with the correlation of Hager *et al.* in 1997,⁵ which depends on the steam superficial velocity, viscosity, specific heat capacity, thermal conductivity, particle diameter, and thermal conductivity. The effective transport properties of the three species of material (dry solid matrix, liquid moisture and vapour) that co-exist within the coal particles were estimated using the method of Looi *et al.*³ and the data were obtained from Perry⁹ and Durie.¹⁰ The temperature increase for this study was smoothly progressive with a highest value of about 470 K. Tar separation was therefore not significant in this case because tar begins to form at about 773 K during low temperature carbonization of coal.⁹ Swelling was also not significant because this phenomenon is a function of rapid heating of coal to eliminate H₂, CH₄, CO, CO₂, C₂–C₄ hydrocarbons, tars, organic compounds, sulphur and nitrogen species.⁹ The simulation was facilitated by using the Flex PDE Version 5.0.19 3D Finite Element software.

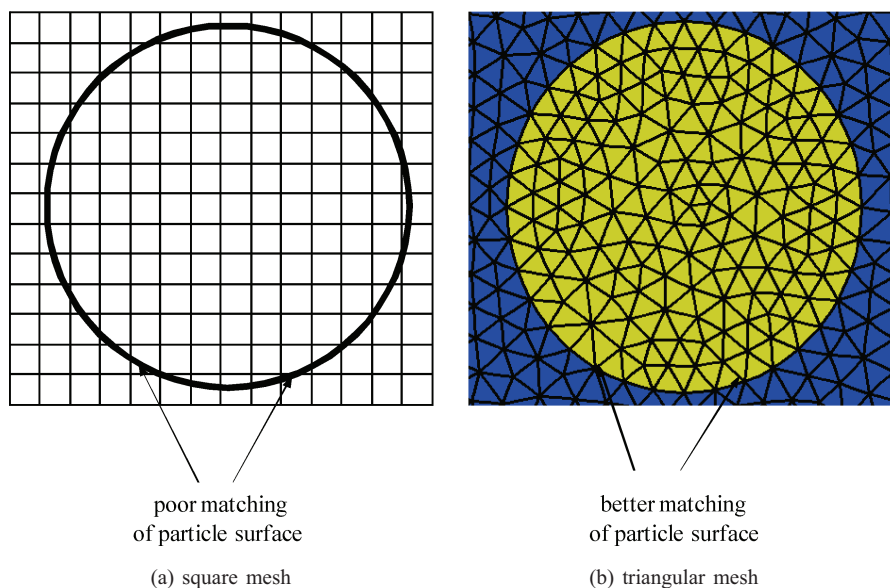


Fig. 2 – Comparison of square mesh and triangular mesh numerical approximations

Results and discussion

The simulated results are presented graphically below as continuous lines, while the experimental data are presented with markers. The triangular markers are for the moisture content, while the circular markers are for the temperature variation of the coal particles.

The experimental result was perfectly matched as may be seen from the plot in Fig. 3. As shown through the model and experimental plots, the particle attained the equilibrium moisture content when the particle temperature almost reached the surrounding steam temperature. However, drying took place for a long period of the operation.

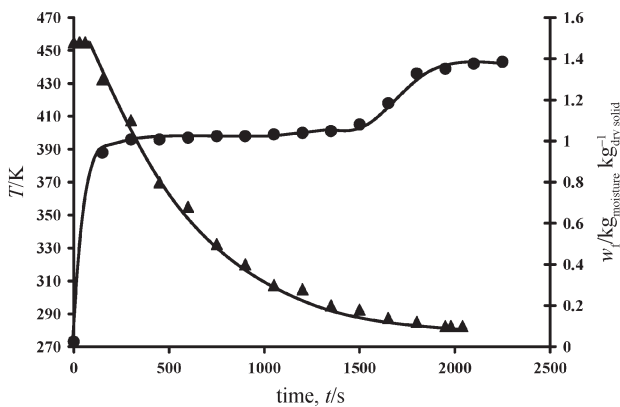


Fig. 3 – Simulation of 12 mm diameter coal particle drying with steam at $2.3 \cdot 10^5$ Pa, 443 K and superficial velocity of 2.7 m s^{-1}

The modelled result perfectly matched the experimental run as may be seen from the plot in Fig. 4. As shown also through the model and experimental plots, the particle attained the equilibrium moisture content when the particle temperature almost reached the surrounding steam temperature.

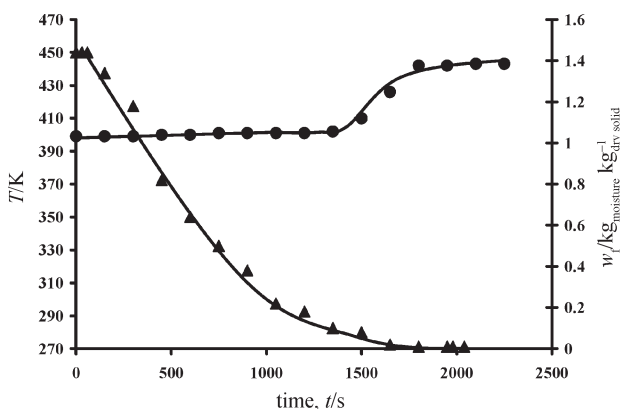


Fig. 4 – Simulation of 12 mm diameter coal particle drying with steam at $2.5 \cdot 10^5$ Pa, 443 K and superficial velocity of 2.7 m s^{-1}

Drying also took place for a long period of the operation. The similarity in observation in Fig. 3 and 4 is the result of the closeness in the operating conditions of the two runs, as well as the reproducibility of results in both the experiment and simulated results.

The modelled result perfectly matched the experimental run as it can be seen from the plot in Fig. 5. The higher pressure operation enabled the drying operation to reach the end point faster than the previous experimental run. The final moisture content also seems to be higher than in the previous experiment, which may be attributed to the forced equilibrium attained due to the higher pressure environment.

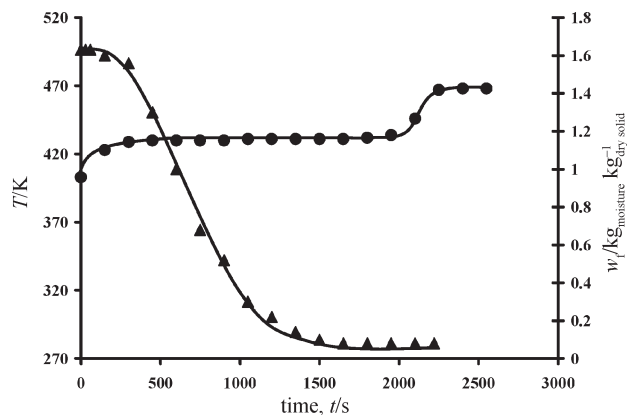


Fig. 5 – Simulation of 12 mm diameter coal particle drying with steam at $5.8 \cdot 10^5$ Pa, 468 K and superficial velocity of 1.5 m s^{-1}

The modelled result perfectly matched the experimental run as may be seen from the plot in Fig. 6. The much higher pressure operation enabled the drying operation to reach end point even faster than the previous experimental run. The final moisture content was higher than in the previous experiment,

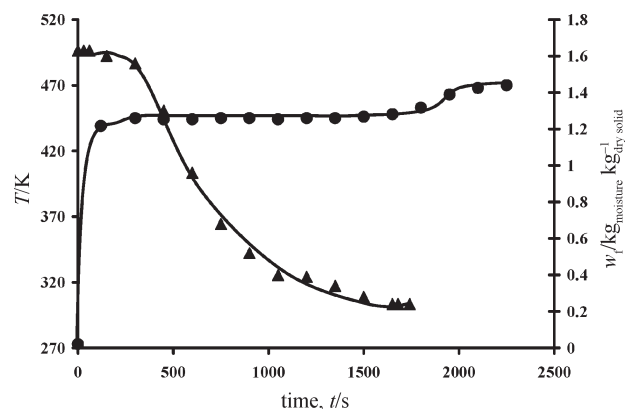


Fig. 6 – Simulation of 12 mm diameter coal particle drying with steam at $8.4 \cdot 10^5$ Pa, 470 K and superficial velocity of 1.4 m s^{-1}

which may be attributed to the more forceful equilibrium attained due to the higher pressure environment.

Fig. 7 depicts a very good match between simulated and experimental results also. The lower bulk steam temperature however shows the less steep slope depicted from the initial particle temperature to the final particle temperature. The final moisture content also took a longer period to be attained.

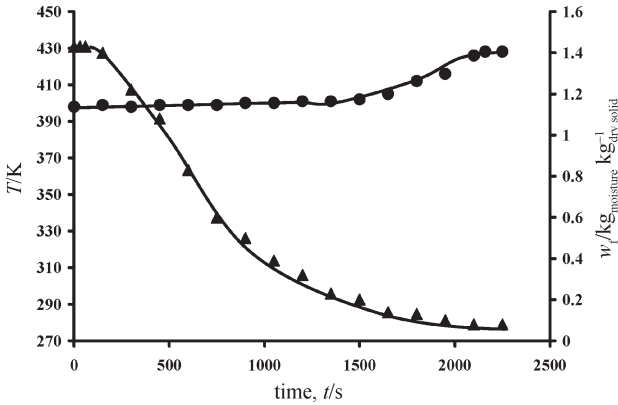


Fig. 7 – Simulation of 12 mm diameter coal particle drying with steam at $2.5 \cdot 10^5$ Pa, 428 K and superficial velocity of 2.8 m s^{-1}

In addition to the perfectly matched trend observed in Fig. 8, the effect of particle diameter on the drying operation was evident with the use of a smaller diameter particle. The particle temperature rose early, while the final moisture content was also attained very fast. These observations confirmed the additional assumptions that were made in the formulation of the model equations for this present work that conductive heat transfer within the particle has a significant effect on the heat transfer and drying rate, due to the faster receding drying core and the faster shrinking effect more pronounced in a smaller particle.

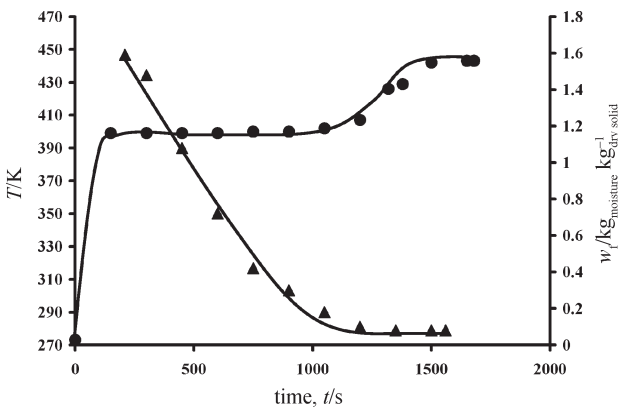


Fig. 8 – Simulation of 10 mm diameter coal particle drying with steam at $2.4 \cdot 10^5$ Pa, 443 K and superficial velocity of 2.7 m s^{-1}

The pronounced effect of high pressure steam is shown in Fig. 9. The particle temperature increased very fast, while the drying also completed in a short period. This was also confirmed with the simulation plot. The faster drying operation is simply due to the fact that the hot steam approaches the particle faster due to the high superficial velocity stream, and also conveys the wet stream away faster, paving the way for equilibrium to be attained faster.

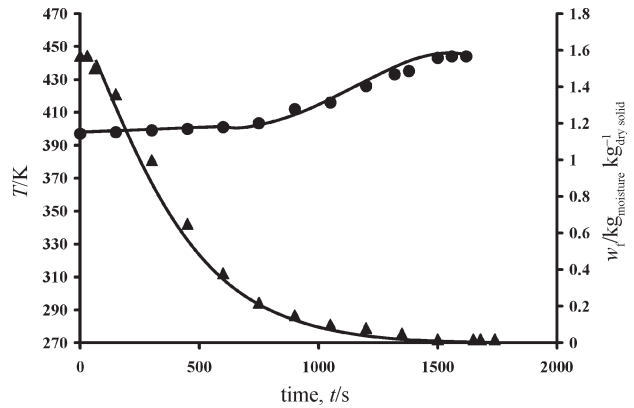


Fig. 9 – Simulation of 12 mm diameter coal particle drying with steam at $2.3 \cdot 10^5$ Pa, 444 K and superficial velocity of 3.5 m s^{-1}

Fig. 10 shows a good match between modelled and experimental values. The slower drying operation depicted is a reflection of the lower velocity operation relative to that of Fig. 9, even though the pressure and surrounding steam temperature are almost similar.

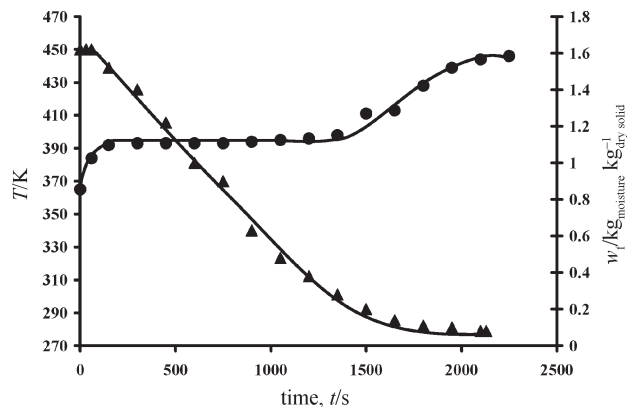


Fig. 10 – Simulation of 12 mm diameter coal particle drying with steam at $2.0 \cdot 10^5$ Pa, 446 K and superficial velocity of 2.7 m s^{-1}

Fig. 11 is another plot that showed the reliability of the proposed model. Using similar operational parameters to those in Fig. 7, the reproducibility of results is once again displayed in this

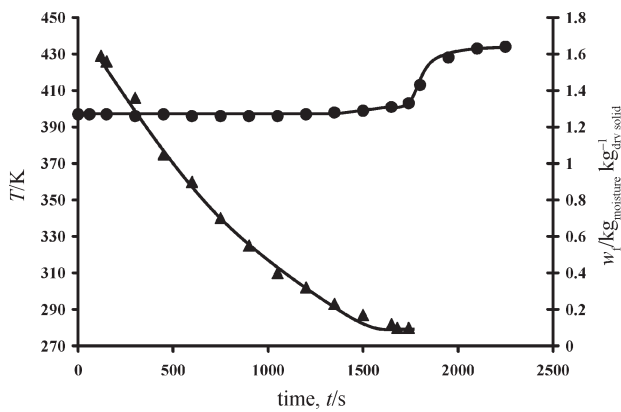


Fig. 11 – Simulation of 12 mm diameter coal particle drying with steam at $2.3 \cdot 10^5$ Pa, 434 K and superficial velocity of 2.7 m s^{-1}

figure. The drying operation ended at almost the same time.

Conclusions

Percentage deviation from experimental results did not exceed + 8 % and –7 % for all the simulated results. The suitability of the proposed and validated model in this work further confirmed the issue of the receding core model as well as particle shrinkage, which has been a subject of controversy among researchers in this field for many years that their effect cannot be overemphasised. Furthermore, the model presented in this work is a good predictive tool for better design and operation of a superheated steam dryer for drying coal in future.

List of symbols

A_f	– area of the drying front, m^2
c_p	– specific heat capacity, $\text{J kg}^{-1} \text{K}^{-1}$
h	– heat transfer coefficient, $\text{W m}^{-2} \text{K}^{-1}$
h_{lg}	– latent heat of evaporation of steam, J kg^{-1}
J	– heat flux, W m^{-2}
k	– heat conductance, W K^{-1}
m_s	– mass of dry coal particle, kg
q_w	– rate of evaporation of moisture at the drying front, $\text{kg m}^{-2} \text{s}^{-1}$
r	– varying particle radius, m
r_p	– particle radius, m

r_f	– radius of drying front, m
r_t	– transient particle radius, m
t	– time of drying, s
T	– transient particle temperature, K
T_h	– temperature of hot surrounding air, K
T_s	– saturated temperature of steam, K
V_i	– initial particle volume, m^3
V_f	– final particle volume, m^3
V_t	– transient particle radius, m^3
ΔV	– change in particle volume, m^3
w_i	– initial moisture content, $\text{kg moisture kg}^{-1} \text{dry solid}$
w_f	– final moisture content, $\text{kg moisture kg}^{-1} \text{dry solid}$
w_t	– transient moisture content, $\text{kg moisture kg}^{-1} \text{dry solid}$
z	– height, m

Greek symbols

κ	– thermal conductivity, $\text{W m}^{-1} \text{K}^{-1}$
ρ	– density, kg m^{-3}
ρ_l	– moisture density, kg m^{-3}
μ	– viscosity, $\text{kg m}^{-1} \text{s}^{-1}$

References

- Hausbrand, E., *Drying by Means of Air and Steam*, 3rd Revised English Edition, Scott Greenwood and Sons, London, 1924.
- Karrer, J., *Drying with Superheated Steam*, Schweizerische Bauzeitung, 1920, pp. 228–230.
- Looi, A. Y., Golonka, K., Rhodes, M., *Chemical Engineering Journal* **87** (2002) 329.
- Edward, K. L., Hugo, S. C., Yao, Z., Wei, Z., Sarunac, N., *Kinetics of Coal Drying in Bubbling Fluidized Beds*, Proceedings Fifth World Congress on Particle Technology, Orlando, Florida, April, 2006, pp 1–6.
- Hager, J., Hermansson, R., Wimmerstedt, R., *Chem. Eng. Sci.* **52** (8) (1997) 1253.
- Shibata, H., Mada, J., Shinohara, H., *Ind. Eng. Chem. Res.* **27** (1988) 2353.
- Khan, J. A., Beasley, D. E., Alatas, B., *Int. J. Heat and Mass Transfer* **34** (1) (1991) 267.
- Moyne, C., Stemmelen, D., Degiovanni, A., *Int. Chem. Eng.* **30** (4) (1990) 654.
- Perry, R. H., Green, D. W. (Eds.), *Perry's Chemical Engineers Handbook*, 7th Edition, McGraw Hill, New York, 1998.
- Durie, R. A. (Ed.), *The Science of Victorian Brown Coal Structure, Properties and Consequences for Utilisation*, Butterworths Heinemann, Oxford, 1991.